A direct comparison between field-measured and sensor-based estimates of soil carbon dioxide flux across six National Ecological Observatory Network sites enabled by the `neonSoilFlux` R package

Ed Ayres   Ridwan Abdi   Natalie Ashburner-Wright
Lillian Brown   Ryan Frink-Sobierajski   Lajntxiag Lee
Dijonë Mehmeti   Christina Tran   Ly Xiong   Zoey Werbin
Naupaka Zimmerman   John Zobitz

1 Abstract

Current estimates of the global terrestrial carbon fluxes between the atmosphere indicate a net sink into soil carbon (not accounting for land use change emissions, Friedlingstein et al. (2023)). A key factor to the uncertainty of the terrestrial carbon sink is quantification of terrestrial soil carbon fluxes, which vary across time and ecosystem type. Robust estimation of soil carbon fluxes on a sub-daily level requires measurements of soil CO_2 concentration, water content, temperature, and other environmental measurements and soil properties. These data are publicly available from the National Ecological Observatory Network at 47 different sites spanning a range of 20 different ecoclimatic domains. We present an R software package (`neonSoilFlux`) that acquires soil environmental data and to computes soil carbon flux at a half-hourly time step at a user-specified NEON site and month in a tidy user format. By design, users with a range of proficiency in the R statistical language can access the `neonSoilFlux` R package. Soil carbon fluxes and associated uncertainties are computed using the flux gradient method via a variety of existing approaches. To validate the computed fluxes, we separately measured soil carbon fluxes with automated sensors at six focal NEON sites. The validation confirmed that a primary challenge in reducing soil carbon flux uncertainty is correctly characterizing diffusivity and soil water content across the soil profile. Outputs from the `neonSoilFlux` package contribute to existing databases of continuous soil carbon measurements, providing near real-time estimates of a critical component to the terrestrial carbon cycle.

2 Introduction

Soils contain the largest reservoir of terrestrial carbon (Jobbágy & Jackson, 2000). A critical component of this reservoir is soil organic matter, the accumulation of which is influenced by biotic factors such as above-ground plant inputs (Jackson et al., 2017). These inputs in turn are influenced by environmental factors such as growing season length, temperature, and moisture (Desai et al., 2022), which also affect the breakdown of soil organic matter and its return to the atmosphere. Across heterogeneous terrestrial landscapes, the interplay between these biotic and abiotic factors influence the size of the soil contribution to the terrestrial carbon sink (Friedlingstein et al., 2023). However, the heterogeneity of these processes across diverse ecosystems in the context of rapid environmental change leads to large uncertainty in the magnitude of this sink in the future, and thus a pressing need to quantify changes in soil carbon pools and fluxes across scales.

Ecological observation networks such as the United States' National Ecological Observatory Network (NEON) and others (e.g. FLUXNET or the Integrated Carbon Observation System) present a significant advancement in the nearly continuous observation of biogeochemical processes at the continental scale. Notably, at 47 terrestrial sites across the continental United States, NEON provides half-hourly measurements of soil CO_2 concentration, temperature, and moisture at different vertical depths. Each of these NEON sites also encompasses measurements of the cumulative sum of all ecosystem carbon fluxes in an airshed using the eddy covariance technique (Baldocchi, 2014). Soil observations provided by NEON are on the same timescale and standardized with eddy covariance measurements from FLUXNET. These types of nearly continuous observational data (NEON and FLUXNET) can be used to reconcile differences between model-derived or data-estimated components of ecosystem carbon flux (Jian et al., 2022; Luo et al., 2011; Phillips et al., 2017; J. Shao et al., 2015; P. Shao et al., 2013; Sihi et al., 2016).

Beyond direct observations of soil CO_2 concentrations and other environmental variables such as moisture or temperature, estimated or observed soil carbon fluxes are a key metric for understanding change in soil carbon pools over time (Bond-Lamberty et al., 2024). A soil carbon flux to the atmosphere (F_S, units μmol m^{-2} s^{-1}), represents the aggregate process of transfer of soil CO_2 to the atmosphere from physical and biological processes (e.g. diffusion and respiration). Measurements of soil carbon fluxes can be coupled with empirical or process models of soil carbon. Soil carbon fluxes can be assumed to encompass soil carbon respiration from autotrophic or heterotrophic sources (Davidson et al., 2006), typically assumed to be static across the soil biome and modeled with a exponential Q_{10} paradigm (Bond-Lamberty et al., 2004; Chen & Tian, 2005; Hamdi et al., 2013).

One method by which F_S is measured in the field is through the use of soil chambers in a closed, well-mixed system (Norman et al., 1997) with headspace trace gas concentrations measured with an infrared gas analyzer (IRGA). F_S can also be estimated from soil CO_2 measurements at different depths in the soil using the flux-gradient method (Maier & Schack-Kirchner, 2014). This method is an approach that uses conservation of mass to calculate flux at a vertical soil

depth z at steady state by applying Fick's law of diffusion. A simplifying assumption for the flux-gradient method is that there is no mass transfer in the other spatial dimensions x and y (Maier & Schack-Kirchner, 2014). The diffusivity profile, a key component of this calculation, varies across the soil depth as a function of soil temperature, soil volumetric water content, atmospheric air pressure, and soil bulk density (Millington & Shearer, 1971; Moldrup et al., 1999; Sallam et al., 1984).

Databases such as the Soil Respiration Database (SRDB) or the Continuous Soil Respiration Database (COSORE) add to the growing network of resources for making collected observations of soil fluxes available to other workers (Bond-Lamberty, 2018; Bond-Lamberty et al., 2020; Bond-Lamberty & Thomson, 2010; Jian et al., 2021; Jiang et al., 2024). However, these databases currently encompass primarily direct soil measurements of fluxes (i.e. those using methods like the closed-chamber method described above). Currently, NEON provides all measurements to calculate F_S from Fick's law, but soil flux as a derived data product was descoped from the initial network launch due to budget constraints (Berenbaum et al., 2015). Deriving estimates of F_S using continuous sensor data across NEON sites thus represents a high priority.

This study describes an R software package, `neonSoilFlux`, that can be used to derive a standardized estimate of F_S at all terrestrial NEON sites. After calculating these flux estimates, we then validated them against direct chamber-based field observations of soil carbon dioxide flux from a subset of terrestrial NEON sites spanning six states.

Key objectives of this study are to:

1. Apply the flux-gradient method to estimate soil CO_2 flux from continuous sensor measurements across NEON sites.
2. Benchmark estimated soil carbon fluxes against field measurements (e.g. direct measurements of soil flux).
3. Identify sources of error in the flux-gradient approach across diverse sites in order to guide future work.

3 Materials and Methods

3.1 Field methods

3.1.1 Focal NEON Sites

In order to acquire field data to validate model predictions of flux, we selected six terrestrial NEON sites for analysis. We conducted field measurement campaigns at these sites, which span a range of environmental gradients and terrestrial domains (Table 1). SJER, SRER, and WREF were visited during May and June of 2022, and WOOD, KONZ, and UNDE during May and June of 2024.

Over the course of two field campaigns in 2022 and 2024, we conducted week-long visits at each site. In consultation with NEON field staff, we first selected a specific plot in the soil sampling array to maximize the concurrent availability of sensor data. We then made measurements of flux on an hourly or half-hourly interval for 8 hours each day after letting temporarily-installed soil collar(s) equilibrate for approximately 24 hours.

Table 1: Listing of NEON sites studied for field work and analysis. $\overline{T_S}$: average soil temperature during field measurements. $\overline{SWC}$: average soil water content during field measurements. Soil plot refers to the particular location in the soil sensor array (denoted as HOR by NEON) where field measurements were made.

Site (NEON site ID)	Location	Ecosystem type	Mean annual temperature	$\overline{T_S}$ (°)	Mean annual precipitation	$\overline{SWC}$ (%)	Field measurement dates	Soil plot
Santa Rita Experimental Range (SRER)	31.91068, -110.83549	Shrubland	19.3°C	47.6°	346 mm	4.0%	29 May 2024 - 01 June 2024	004
San Joaquin Experimental Range (SJER)	37.10878, -119.73228	Oak woodland	16.4°C	41.7°	540 mm	1.2%	01 June 2022 - 04 June 2022	005
Wind River Experimental Forest (WREF)	45.82049, -121.95191	Evergreen forest	9.2°C	15.3°	2225 mm	27.2%	07 June 2022 - 09 June 2022	001
Chase Lake National Wildlife Refuge (WOOD)	47.1282, -99.241334	Restored prairie grassland	4.9°C	14.9°	495 mm	14.9%	03 June 2024 - 09 June 2024	001
Konza Prairie Biological Station (KONZ)	39.100774, -96.563075	Tallgrass Prairie	12.4°C	23.4°	870 mm	23.4%	29 May 2024 - 01 June 2024	001
University of Notre Dame Environmental Research Center (UNDE)	46.23391, -89.537254	Deciduous forest	4.3°	13.0°	802 mm	13.0%	22 May 2024 - 25 May 2024	004

3.1.2 Soil collar placement

Either one (2022 sampling campaign) or two (2024 sampling campaign) PVC soil collars (FIXME: diameter) were installed in close proximity to the permanent NEON soil sensors at each site. The soil plot where measurements were taken was chosen at each site in consultation with NEON staff to maximize likelihood of quality soil sensor measurements during the duration of the IRGA measurements at each site.

IN PROGRESS: Add graphic of soil plot layout and placement of soil collar(s) – could make diagram in OmniGraffle?

3.1.3 Infrared gas analyzer measurements of soil CO_2 flux

During the summer 2022 field campaign, a LI-COR 6800 with soil flux chamber attachment was used to measure soil fluxes for 8 hours each day on an hourly interval. During the summer 2024 field campaign, the LI-6800 measurements were taken on a half-hourly interval and were paired with an automated soil flux chamber setup (FIXME multiplexer, IRGA, chamber model numbers) that made automated measurements on a half-hourly interval 24 hours a day while we were on site. Each instrument was paired with a soil temperature and moisture probe (FIXME: Stevens model #) that was used to make soil temperature and moisture measurements concurrent with the CO_2 flux measurements.

IN PROGRESS: Dead bands, measurement duration, instrument self-testing.

3.1.4 Post-collection processing of data

IN PROGRESS: LI-COR SoilFluxPro software to assess dead band and measurement duration.

3.2 `neonSoilFlux` R package

We developed an R package (`neonSoilFlux`; https://CRAN.R-project.org/package=neonSoilFlux) to compute half-hourly soil carbon fluxes and uncertainties from NEON data. The objective of the `neonSoilFlux` package is a unified workflow soil data acquisition and analysis that supplements existing data acquisition software through the `neonUtilities` R package (https://CRAN.R-project.org/package=neonUtilities). Figure 1 outlines the basic workflow of the package.

At a given NEON observation there are five different replicate soil sensor plots, each with measurements of soil CO_2 concentration, soil temperature, and soil moisture at different depths. The `neonSoilFlux` package acquires measured soil water content (National Ecological Observatory Network (NEON), 2024e), soil CO_2 concentration (National Ecological Observatory
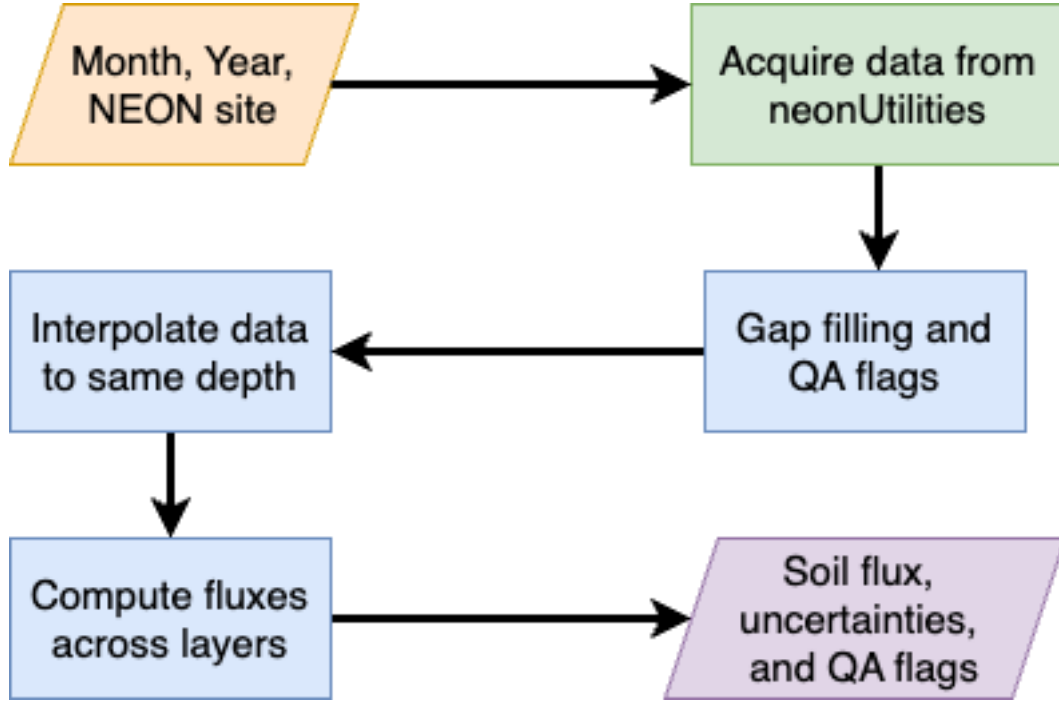
Figure 1: Diagram of `neonSoilFlux` R package. For a given month, year and NEON site (orange parallelogram), the package acquires all relevant data to compute F_S using the `neonUtilities` R package (green rectangle). Data are gap-filled according to reported QA flags and interpolated to the same measurement depth before computing the soil flux, uncertainties, and final QA flags (blue rectangles). The package reports the associated soil flux, uncertainties, and quality assurance (QA) flags for the user (purple parallelogram).

Network (NEON), 2024b), barometric pressure from the nearby tower (National Ecological Observatory Network (NEON), 2024a), soil temperature (National Ecological Observatory Network (NEON), 2024d), and soil properties (e.g. bulk density) (National Ecological Observatory Network (NEON), 2024c). The static soil properties were collected from a nearby soil pit during site characterization and are assumed to be constant at each site.
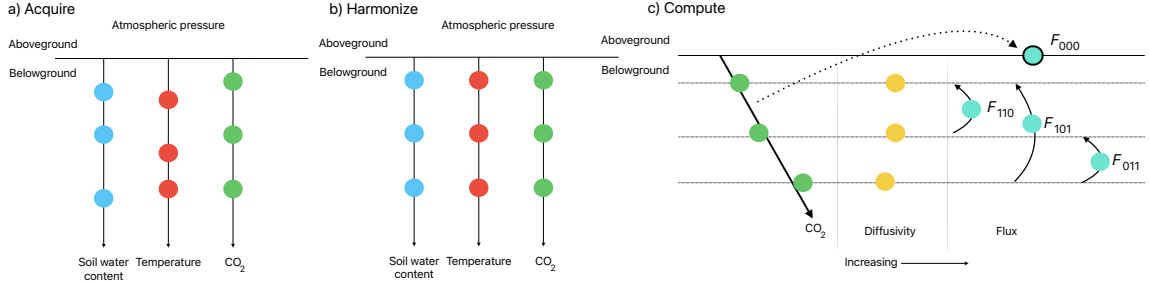

Figure 2: Model diagram for data workflow for the `neonSoilFlux` R package. a) Acquire: Data are obtained from given NEON location and horizontal sensor location, which includes soil water content, soil temperature, CO_2 concentration, and atmospheric pressure. All data are screened for quality assurance, with gap-filling of missing data reported. b) Any belowground data are then harmonized to the same depth as CO_2 concentrations using linear regression. c) The flux across a given depth is computed via Fick's law, denoted with F_{ijk}, where i, j, or k are either 0 or 1 denoting the layers the flux is computed across (i = closest to surface, k = deepest). F_{000} represents a flux estimate where the gradient dC/dz is the slope of a linear regression of CO_2 with depth.

The workflow to computing a value of F_S with the `neonSoilFlux` consists of three primary steps, illustrate in Figure 2. First, NEON data are acquired for a given site and month via the `neonUtilities` R package (yellow parallelogram and green rectangle in Figure 1 and Panel a in Figure 2). Acquired environmental data can be exported to a comma separated value file for additional analysis. Quality assurance (QA) flags with an observation are reported as an indicator variable.

The next step is harmonizing the data to compute soil fluxes across soil layers. This step consists of three different actions (blue rectangles in Figure 1 and Panel b in Figure 2). If a given observation by NEON is reported as not passing a quality assurance check, we applied a gap filling method to replace that measurement with its monthly mean at that same depth (Section 3.2.1). Belowground measurements of soil water and soil temperature are then interpolated to the same depth as soil CO_2 measurements. The diffusivity (Section 3.2.2) and soil flux across different soil layers (Section 3.2.3) are then computed.

The final step is computing a surface soil flux through extrapolation to the surface (purple parallelogram in Figure 1 and Panel c in Figure 2). Uncertainty on a soil flux measurement is

computed through quadrature. An aggregate quality assurance (QA) flag for each environmental measurement is also reported, representing if any gap-filled measurements were used in the computation of a soil flux. Within the soil flux-gradient method, several different approaches can be used to derive a surface flux (Maier & Schack-Kirchner, 2014); the `neonSoilFlux` package reports four different possible values of soil surface flux (Section 3.2.3).

3.2.1 Gap-filling routine

NEON reports QA flags as a binary value for a given measurement and half-hourly time. We replaced any flagged measurements at a location's spatial depth z with a bootstrapped sample of the monthly mean for all un-flagged measurements for that month. These measurements are represented by the vector $\mathbf{m}$, standard errors σ, and the 95% confidence interval (the so-called expanded uncertainty, Farrance & Frenkel (2012)) ϵ. All of these vectors have length M. We have that $\vec{\sigma}_i \leq \vec{\epsilon}_i$. We define the bias as $\mathbf{b} = \sqrt{\epsilon^2 - \sigma^2}$.

We generate a vector of bootstrap samples of the distribution of the monthly mean $\overline{m}$ and monthly standard error $\overline{\sigma}$ the following ways:

1. Randomly sample from the uncertainty and bias independently: σ_j and the bias $\mathbf{b}_k$ (not necessarily the same sample).
2. Generate a vector $\mathbf{n}$ of length N, where $\mathbf{n}_i$ is a random sample from a normal distribution with mean m_i and standard deviation σ_j. Since $M < N$, values from $\mathbf{m}$ will be reused.
3. With these N random samples, $\overline{y}_i = \overline{\overline{x}} + \vec{b}_k$ and s_i is the sample standard deviation of $\vec{x}$. We expect that $s_i \approx \vec{\sigma}_j$.
4. The reported monthly mean and standard deviation are then computed $\overline{\overline{y}}$ and $\overline{s}$. Measurements and uncertainties that did not pass the QA check are then substituted with $\overline{\overline{y}}$ and $\overline{s}$.

This gap-filling method described here provides a consistent approach for each data stream, however we recognize that other gap-filling alternatives may be warranted for longer-term gaps (e.g. such as correlations with other NEON measurement levels and soil plots), or measurement specific gap-filling routines. We discuss the effect of gap-filling on our measurements in Section 5.

3.2.2 Soil diffusivity

Soil diffusivity D_a at a given measurement depth is the product of the diffusivity in free air $D_{a,0}$ (m^2 s^{-1}) and the tortuosity ξ (no units) (Millington & Shearer, 1971).

We compute $D_{a,0}$ with Equation 1:

$$D_{a,0} = 0.0000147 \cdot \left(\frac{T_i + 273.15}{293.15}\right)^{1.75} \cdot \left(\frac{P}{101.3}\right) \tag{1}$$

where T_i is soil temperature (°C) at depth i (National Ecological Observatory Network (NEON), 2024d) and P surface barometric pressure (kPa) (National Ecological Observatory Network (NEON), 2024a).

Previous studies by Sallam et al. (1984) and Tang et al. (2003) demonstrated the sensitivity of modeled F_S depending on the tortuousity model used to compute diffusivity. At low soil water content, the choice of tortusoity model may lead to order of magnitude differences in D_a, which in turn affect modeled F_S. The `neonSoilFlux` package uses two different models for ξ. representing the extremes reported in Sallam et al. (1984). The first approach uses the Millington-Quirk model for diffusivity, Equation 2 (Millington & Shearer, 1971):

$$\xi = \frac{(\phi - SWC_i)^{10/3}}{\phi^2} \tag{2}$$

In Equation 2, SWC is the soil water content at depth i (National Ecological Observatory Network (NEON), 2024e) and ϕ is the porosity (Equation 3), which in turn is a function of soil physical properties (National Ecological Observatory Network (NEON), 2024c):

$$\phi = \left(1 - \frac{\rho_s}{\rho_m}\right)(1 - f_V) \tag{3}$$

In Equation 3, ρ_m is the particle density of mineral soil (2.65 g cm^{-3}), ρ_s the soil bulk density (g cm^{-3}) excluding coarse fragments greater than 2 mm (National Ecological Observatory Network (NEON), 2024c). The term f_V is a site-specific value that accounts for the proportion of soil fragments between 2-20 mm. Soil fragments greater than 20 mm were not estimated due to limitations in the amount of soil that can be analyzed (National Ecological Observatory Network (NEON), 2024c). We assume there are no pores within rocks.

The second approach to calculate ξ is the Marshall model (Marshall, 1959), where $\xi = \phi^{1.5}$, with ϕ defined from Equation 3.

3.2.3 Soil flux computation

We applied Fick's law (Equation 4) to compute the soil flux F_{ij} (μmol m^{-2} s^{-1}) across two soil depths i and j:

$$F_{ij} = -D_a \frac{dC}{dz} \tag{4}$$

where D_a is the diffusivity (m^2 s^{-1}) and $\frac{dC}{dz}$ is the gradient of CO_2 molar concentration (μmol m^{-3}, so the gradient has units of μmol m^{-3} m^{-1}). The soil surface flux is theoretically defined by applying Equation 4 to measurements collected at the soil surface and directly below the surface. Measurements of soil temperature, soil water content, and soil CO_2 molar

concentration across the soil profile allow for application of Equation 4 across different soil depths. Each site had three measurement layers, so we denote the flux between which two layers as a three-digit subscript F_{ijk} with indicator variables i, j, and k indicate if a given layer was used (written in order of increasing depth), according to the following:

- F_{000} is a surface flux estimate using the intercept of the linear regression of D_a with depth and the slope from the linear regression of CO_2 with depth (which represents $\dfrac{dC}{dz}$ in Fick's Law). Tang et al. (2003) used this approach to compute fluxes in an oak-grass savannah.
- F_{110}, F_{011} are fluxes across the two most shallow layers and two deepest layers respectively. The diffusivity used in Fick's Law is always at the deeper measurement layer. When used as a surface flux estimate we assume CO_2 remains constant above this flux depth.
- F_{101} is a surface flux estimate using linear extrapolation using concentration measurements between the shallowest and deepest measurement layer. Hirano et al. (2003) and Tang et al. (2005) used an approach similar to F_{101} in a temperate deciduous broadleaf forest and ponderosa pine forest respectively.

Uncertainty in all F_{ijk} is computed through quadrature (Taylor, 2022).

3.3 Post processing evaluation

Following collection of field measurements from the LICOR and calculation of the soil fluxes from `neonSoilFlux` package, we compared measured F_S (from the LICOR instruments) to a given soil flux calculation `neonSoilFlux` for each site and flux computation method. Statistics included the associated R^2 value, root mean squared error (RMSE), and signal to noise ratio (SNR), defined as the ratio of a modeled soil flux (F_{ijk}) from `neonSoilFlux` to its quadrature uncertainty (σ_{ijk}).

We observed that the range of values (e.g. $F_{ijk} \pm \sigma_{ijk}$ was much larger than the measured field flux. We evaluated $|F_S - F_{ijk}| < (1 - \epsilon)\sigma_{ijk}$, where F_S is a measured field soil flux from the LICOR 6800 (the LICOR 8250 was used at only three sites). The parameter ϵ was an uncertainty reduction factor to evaluate how much the quadrature uncertainty could be reduced while maintaining precision between modeled F_{ijk} and measured F_S.

Finally, for a half-hourly interval we also computed a *post hoc* D_a using the LICOR flux along with the CO_2 surface gradient reported by NEON using the measurement levels closest to the surface.

4 Results

Figure 3 reports the timeseries of out the measured fluxes from the LICOR 6800 and 8250 compared to modeled soil fluxes from the `neonSoilFlux` R package. Figure 4 and and computed fluxes and uncertainty at each measurement site. Results are reported in local time. Positive values of the flux indicate that there is a flux moving towards the surface. For ease of clarity the fluxes at F_{111} and F_{000} are only shown in the top row (surface), followed by the fluxes at individual separate layer (F_{100}, F_{010}, F_{001}). Overall, with the exception of WREF and SRER (discussed later) the computed fluxes were on the same order of magnitude and timing as the measured field fluxes.
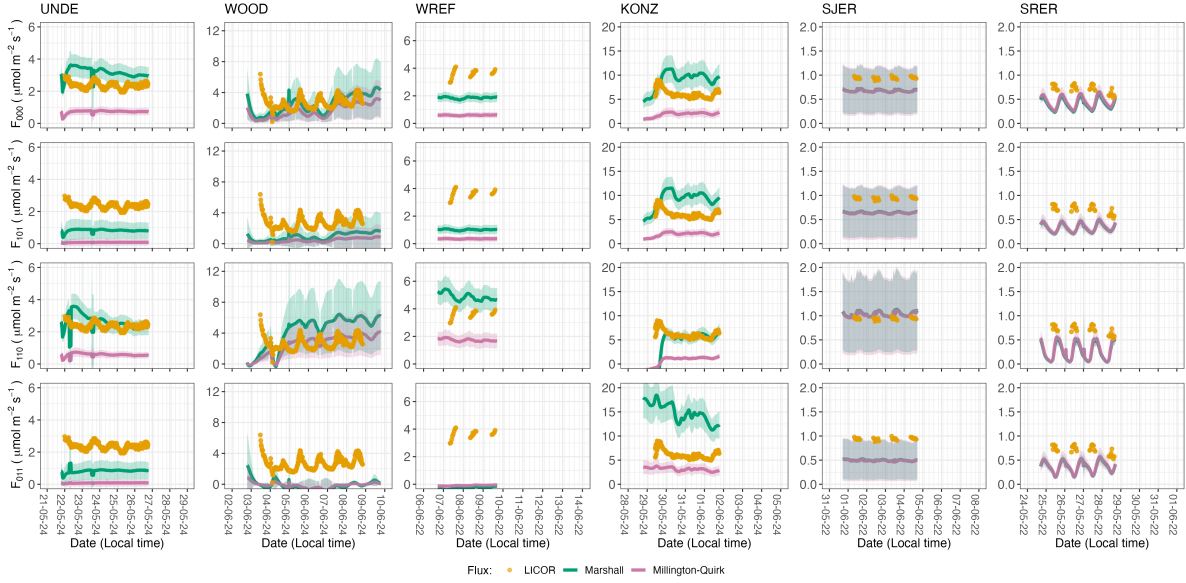

Figure 3: Timeseries of both measured F_S (yellow circles) and modeled soil fluxes (green or purple lines) by the `neonSoilFlux` R package. Fluxes from the `neonSoilFlux` R package are separated by the diffusivity model used (Millington-Quirk or Marshall, Section 3.2.2). Vertical axis labels in the first column represent the measurement levels where the flux-gradient approach is applied (Section 3.2.3). Ribbons for modeled soil fluxes represent $\pm$ 1 standard deviation. Results are reported in local time.

RESULTS TO INCLUDE: TABLE OF STATS (R2, RMSE)

Figure 5 reports the usage of gap-filled environmental measurement types (which could be one CO_2, SWC, or T_S at any measurement depth, and also including P) to compute F_S. Panel a) reports the proportion of gap-filled values for an environmental measurement at each site and Panel b) displays the distribution of gap-filled measurements at each site. The largest contribution to gap-filled measurements was soil water. SJER and WOOD utilized the largest number of gap-filled measurements, which were primarily SWC and T_S.
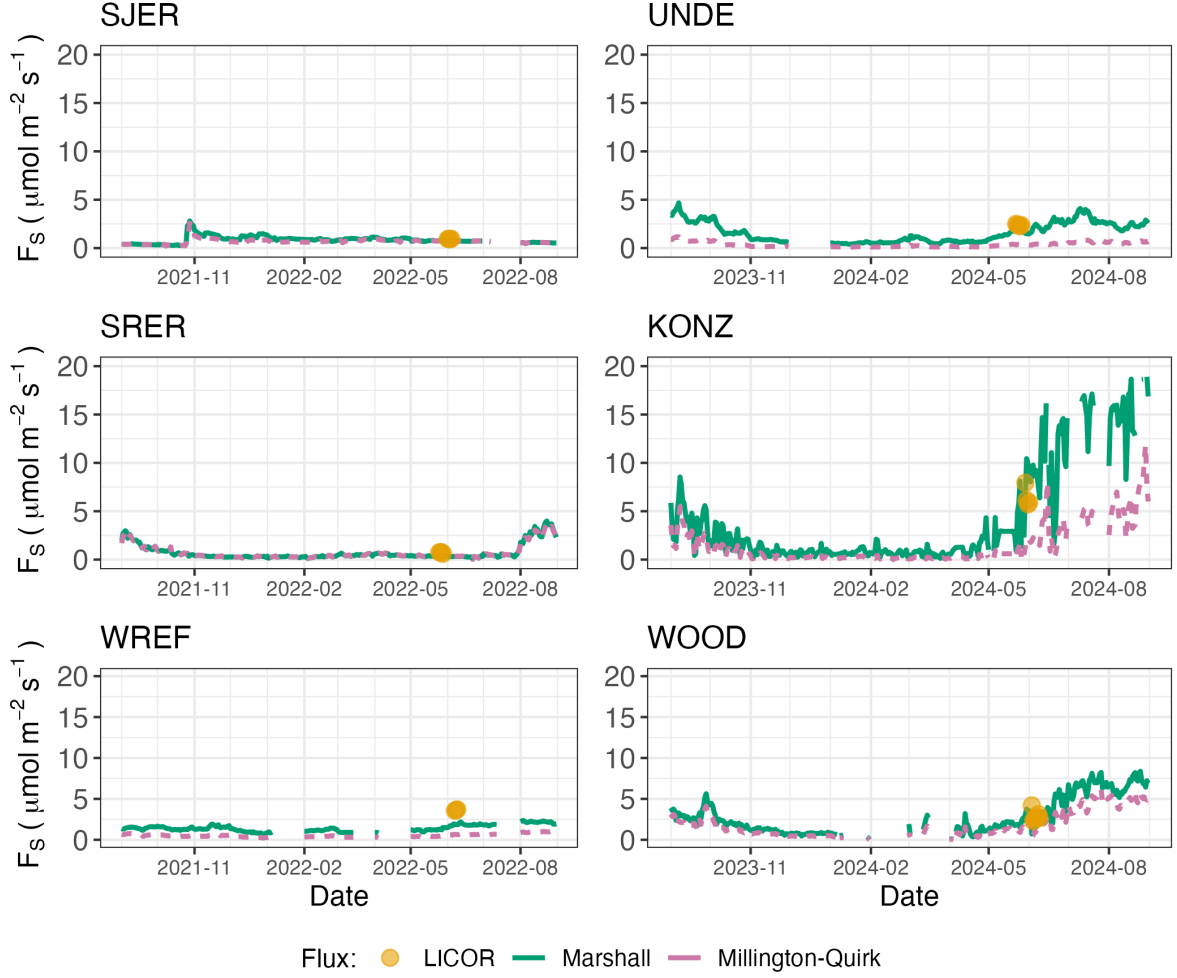
11

Figure 4: Timeseries of both daily-averaged field F_S (yellow circles) and daily ensemble averaged soil fluxes (green or purple lines) by the `neonSoilFlux` R package, separated by the diffusivity model used (Millington-Quirk or Marshall, Section 3.2.2). The timeseries of modeled fluxes are a daily ensemble average of all flux-gradient approaches (F_{000}, F_{101}, F_{011}, F_{110}, Section 3.2.3).
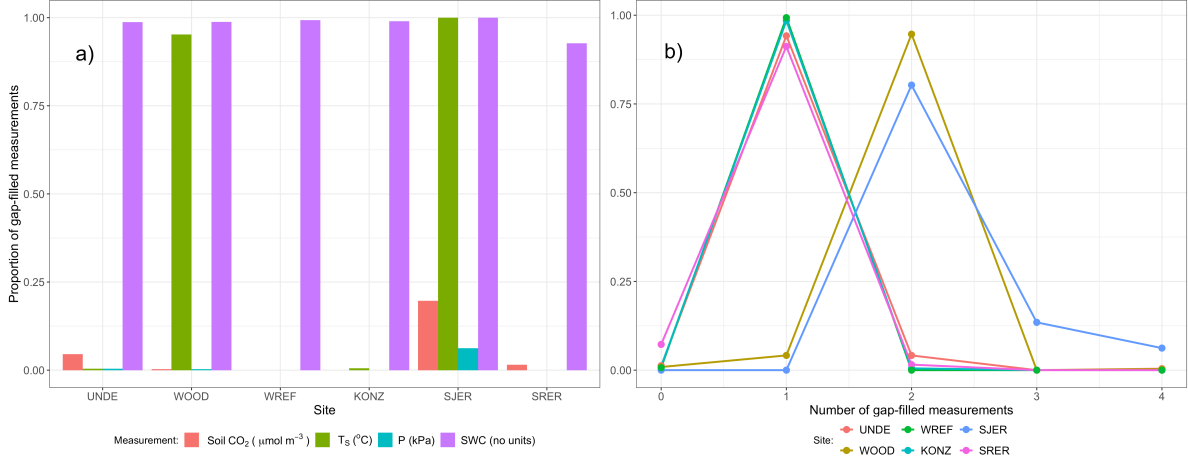
Figure 5: Panel a) Proportion of gap-filled environmental measurements used to generate F_S from the `neonSoilFlux` package, by study site. Panel b) distribution of the usage of gap-filled measurements at each site.

Figure: flux results at the different levels (000,111,001,010,100) Diffusivity at the different levels for comparison (also include derived diffusivity?) Stats at the different levels (with the lags)

Figure 6 reports both the computed SNR and the proportion of measured field fluxes within the modeled uncertainty for a given flux computation method F_{ijk} (Section 3.3). Here, values of SNR greater than unity indicates a reported uncertainty is smaller, propogated by quadrature from a relatively higher precision from measured input variables (CO_2, T_S, SWC, or P). The sensitivity to the uncertainty reduction factor (ϵ, bottom panels in Figure 6) demonstrates how accuracy could be improved if modeled uncertainty σ_{ijk} decreases.

Figure 7 reports the distribution of D_a (from both the Marshall and Millington-Quirk methods, Section 3.2.2) at each study site, and the *post hoc* computed D_a (@. For comparison, for a half-hourly interval we also computed a *post hoc* D_a using the LICOR flux along with the CO_2 surface gradient reported by NEON using the measurement levels closest to the surface.

5 Discussion

This study presents a unified data science workflow to efficiently process automated measurements of belowground soil CO_2 concentrations, water, and temperature to infer estimates of soil surface CO_2 effluxes through application of Fick's Law (Equation 4). Our core goals in this study were: (1) to generate estimates of soil flux from continuous soil sensor data at terrestrial NEON sites using the flux-gradient method and then (2) to compare those estimates to field-measured fluxes based on the closed chamber approach at six NEON focal sites. We discuss
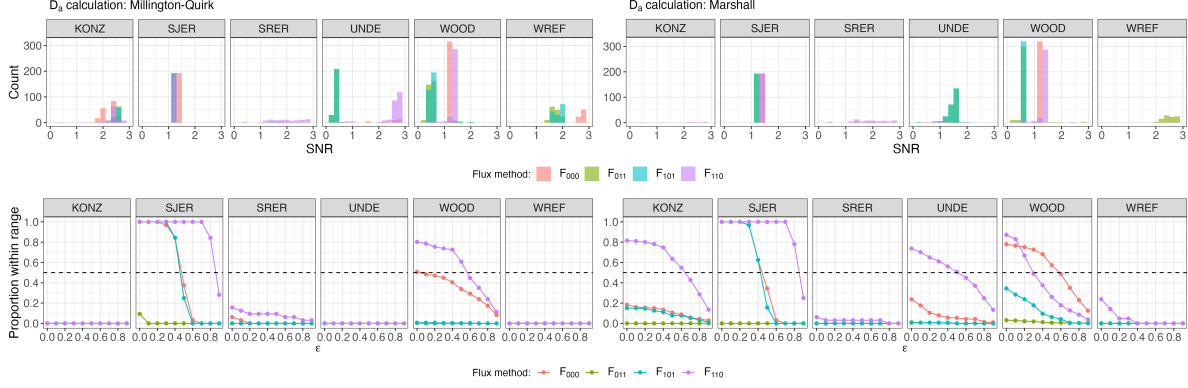
Figure 6: Top panels: distribution of SNR values across each of the different sites for modeled effluxes from the `neonSoilFlux` package, depending on the diffusivity calculation used (Millington-Quirk or Marshall, Section 3.2.2). Bottom panels: Proportion of measured F_S within the modeled range of a flux computation method F_{ijk} given an uncertainty reduction factor ϵ, or $|F_S - F_{ijk}| < (1 - \epsilon)\sigma_{ijk}$.
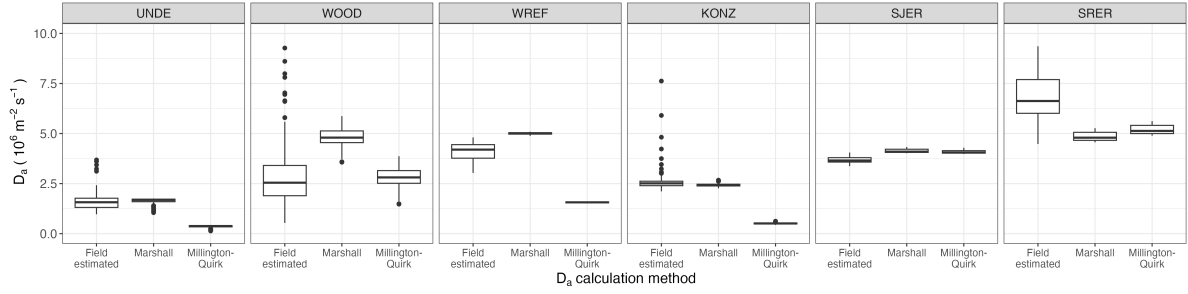

Figure 7

14

our progress toward these core goals through (1) an overall evaluation of the flux-gradient approach (and uncertainty calculation) and (2) site-specific evaluation of differences in estimated vs measured fluxes.

5.1 General evaluation of flux-gradient approach

Key assumptions of the flux-gradient approach are that CO_2 concentrations increase throughout the soil profile. We found that this condition was met at XXX% across the study period. Periods where this gradient condition are not met generally are connected to biophysical processes such soil wetting events (e.g. KONZ), which have the effect of temporarily reducing the soil respiration or efflux. For modeling soil respiration, typically a non-linear response function is considered, that also considers soil type as well (Bouma & Bryla, 2000; Yan et al., 2016, 2018). For the `neonSoilFlux` package soil type is connected to the bulk density, which is separately determined / measured at a site.

The largest source of uncertainty to improve reliability of the flux estimate is to prevent the usage of gap-filled data, especially with soil water (Figure XXX). Across the observed half-hourly periods for field measurements, the percentage of half-hourly periods where all four environmental measurements were available spanned from 0% (SJER) to 7% (SRER), but three sites (WREF, SRER, UNDE) had 95% of half-hourly intervals with just one gap-filled measurement.Where appropriate we have replaced measurements flagged to the protocol with a monthly gap-filled value. Further extensions of the gap filling method could use more sophisticated gap-filling routines, similar to what is used for net ecosystem carbon exchange (Falge et al., 2001; Liu et al., 2023; Mariethoz et al., 2015; Moffat et al., 2007; Zhang et al., 2023).

We recognize that this gap-filling approach may lead to gap-filled values that arebut somewhere we need to say that this this approach may lead to gap-filled values that are quite different from the actual values. For example, it would probably underestimate soil moisture if a rain event has just occurred, right? Also, since it doesn't appear to account for time of day, nighttime soil temperature would probably be overestimated, whereas the opposite would be true for daytime. It probably works fine for pressure. Maybe say that other gap filling options could be explored in the future, e.g., I'm involved in developing a National Coordinated Soil Moisture Monitoring Network data quality document that suggests that soil moisture gaps shorter than 5 hours be gap-filled via linear interpolation (it hasn't been published yet). . Maybe justify the current approach by saying it provides a consistent approach that can be applied to each data stream, but further work may explore alternative gap-filling approaches.

Based on this approach, we would *a priori* expect $F_{011} \leq F_{101} \leq\leq F_{110} \leq F_{000}$ because the previous flux estimates ones correspond to deeper depths which will could miss CO_2 produced in shallower layers. Additionally, field flux measurements should correlate with F_{000} because they represent surface fluxes.

Diffusivity taken from the megapit. Big microsite and temporal differences, soil shrink / swell. How do we think about what that means for using this approach to generalize across a NEON site over continuous time.

- Back calculation of bulk density to NEON sites (boxplot figure).

5.2 Evaluation of flux-gradient approach at each site

Figure 6 illustrates the tradeoff between accuracy for modeled fluxes (defined here as closeness to field-measured F_S) and precision defined by the SNR, and how this is confounded by the choice of diffusivity model used. MORE HERE

The six sites studied provide separate case studies for considerations when applying the flux-gradient method to evaluate resulting uncertainties and fluxes.

SRER is characterized by sandy soil, which also led to the hottest site there. Fluxes are driven by the change and response to temperature in the temperature driven, whereas we observed a decoupling of temperature across the different layers (supplementary figures?) For this instance, using the flux across the top two layers (F_{110}) produced a pattern of soil flux consistent with the observed field data. The remaining methods F_{101}, F_{011}, or F_{000} are derived from information at the deeper layer, which is decoupled both in terms of temperature and CO_2 concentration.

KONZ is a site that experienced a significant rain event prior to sampling with eventual drying out over the course of the experiment. In this case we observed storage of soil water (as shown in supplementary figures), which increased the soil CO_2 at the top layer, leading to negative values of flux at the start of the experiment, with the fluxes drying out afterwards. In this case only when the soil dried out (or returned to a baseline level), that the fluxes at the provided layer would work out in this case.

WREF experienced an extreme rainfall event in the days preceding field measurements, which meant that flux estimates calculated during the field measurement period sensors relied of gap-filled data. In this case, F_{000} is the better one.

We were able to show that the flux-gradient method produced estimates within XX of the field measured values at X of Y sites.

Tang et al. (2003) noticed a similar pattern in temperature as SRER. Mention alternative diffusivity calculations? (Sallam - but this may not be a factor compared to water availability and gap filling)

When considering systematic deployment of this method across a measurement network, we faced a number of independent challenges for consideration. In developing and validating our approach, we faced a number of challenges related to data availability, including... gap filling, sensor calibration, depth interpolation, rainstorms, etc These errors are all

Derived results from the `neonSoilFlux` package have patterns that are consistent, and comparable, to those directly measured to the field (Figure XXX). The advantage to the `neonSoilFlux` package is the calculation of fluxes across different measurement depths, allowing for additional site-specific customization. Here application of the flux-gradient method provides a baseline estimate of soil fluxes that could be complemented through additional field measurements (e.g. LI-COR).

5.3 Recommendations for future method development

The `neonSoilFlux` package provides three different approaches of values for a soil flux. We believe these approaches reflect a variety of site-specific determination and assumptions used to generate a soil flux measurement (Maier & Schack-Kirchner, 2014), with the choice of method having a determinative approach on reported values. Reported results could further be distilled down using ensemble averaging averaging approaches (Elshall et al., 2018; Raftery et al., 2005).

Figures XXX suggests that the provided uncertainty from `neonSoilFlux` is an overestimate compared to what is actually computed. When $\epsilon = 0$ in Figure Figure 6, that means we are just using the reported uncertainty from neonSoilFlux. Looking at that (epsilon = 0) shows field measurements UNDE, KONZ, SJER are 100% within the reported intervals from neonSoilFlux. But those sites tend to have a SNR < 1, so the uncertainty is pretty noisy. For UNDE, we could even reduce the uncertainty by a factor of 75% (epsilon = 0.75), more than half of the field measurements will still be within the reported intervals. For KONZ, we are still within 70% of the reported intervals when uncertainty is reduced by 90%. That suggests that while the reported accuracy (as compared to field measurements), we do have higher precision.

These challenges notwithstanding, the method used here and made available in the `neonSoilFlux` R package is able to produce nearly continuous estimates of flux across all XXYY terrestrial NEON sites. These estimates are a significant improvement on available approaches to constrain the portion of ecosystem respiration attributable to the soil. This, in turn, aids in our ability to understand the components of net ecosystem flux assessed at these sites using the co-located eddy flux towers.

- Refine estimates to provide a realistic constraint on surface concentration measurements, thereby increasing the gradient.
- Apply machine learning algorithms (e.g. random trees) or model averaging techniques to generate a single flux estimate across each sites spatial location
- Benchmarking flux results to estimates provided by Net ecosystem carbon exchange.

6 Conclusions

We have here presented an R package `neonSoilFlux` for the estimation of soil CO_2 fluxes from continuous buried soil sensor measurements across terrestrial National Ecological Observatory Network sites. We compared the predicted fluxes to those measured directly using a field-based closed chamber approach. We find that...

7 Acknowledgments

8 Conflict of Interest Statements

None declared.

9 Author Contributions

Conceptualization: J.Z., N.Z.; Methodology: E.A, J.Z., N.Z; Software: J.Z., N.Z, Z. W., E. A., D. M., R. A., L. X., L. L.; Validation: J.Z., N.Z.; Formal Analysis: J.Z., N.Z., D. M., R. A., L. X., L. L.; Investigation: J.Z., N.Z., R. F-S., C. T.; Resources: J.Z., N.Z.; Data curation: J.Z., N.Z., D. M., L. X.; Writing – original draft: J.Z., N.Z.; Writing – review and editing: J.Z., N.Z., Z. W., E. A., C. T., D. M., L. X.,; Visualization: J.Z., N.Z., D. M., R. A., L. X.; Supervision: J.Z.; N.Z.; Project Administration: J.Z.; N.Z.; Funding Acquisition: J.Z.; N.Z.

Baldocchi, D. (2014). Measuring fluxes of trace gases and energy between ecosystems and the atmosphere - the state and future of the eddy covariance method. *Global Change Biology*, *20*(12), 3600–3609. https://doi.org/10.1111/gcb.12649

Berenbaum, M. R., Carpenter, S. R., Hampton, S. E., Running, S. W., & Stanzione, D. C. (2015). *Report from the NSF BIO Advisory Committee Subcommittee on NEON Scope Impacts*.

Bond-Lamberty, B. (2018). New Techniques and Data for Understanding the Global Soil Respiration Flux. *Earth's Future*, *6*(9), 1176–1180. https://doi.org/10.1029/2018EF000866

Bond-Lamberty, B., Ballantyne, A., Berryman, E., Fluet-Chouinard, E., Jian, J., Morris, K. A., Rey, A., & Vargas, R. (2024). Twenty Years of Progress, Challenges, and Opportunities in Measuring and Understanding Soil Respiration. *Journal of Geophysical Research: Biogeosciences*, *129*(2), e2023JG007637. https://doi.org/10.1029/2023JG007637

Bond-Lamberty, B., Christianson, D. S., Malhotra, A., Pennington, S. C., Sihi, D., AghaK-ouchak, A., Anjileli, H., Altaf Arain, M., Armesto, J. J., Ashraf, S., Ataka, M., Baldocchi, D., Andrew Black, T., Buchmann, N., Carbone, M. S., Chang, S.-C., Crill, P., Curtis, P. S., Davidson, E. A., … Zou, J. (2020). COSORE: A community database for continuous soil respiration and other soil-atmosphere greenhouse gas flux data. *Global Change Biology*, *26*(12), 7268–7283. https://doi.org/10.1111/gcb.15353

Bond-Lamberty, B., & Thomson, A. (2010). A global database of soil respiration data. *Biogeosciences*, *7*(6), 1915–1926. https://doi.org/10.5194/bg-7-1915-2010

Bond-Lamberty, B., Wang, C., & Gower, S. T. (2004). A global relationship between the heterotrophic and autotrophic components of soil respiration? *Global Change Biology*, *10*(10), 1756–1766. https://doi.org/10.1111/j.1365-2486.2004.00816.x

Bouma, T. J., & Bryla, D. R. (2000). On the assessment of root and soil respiration for soils of different textures: Interactions with soil moisture contents and soil CO2 concentrations. *Plant and Soil*, *227*(1), 215–221. https://doi.org/10.1023/A:1026502414977

Chen, H., & Tian, H.-Q. (2005). Does a General Temperature-Dependent Q10 Model of Soil Respiration Exist at Biome and Global Scale? *Journal of Integrative Plant Biology*, *47*(11), 1288–1302. https://doi.org/10.1111/j.1744-7909.2005.00211.x

Davidson, E. A., Janssens, I. A., & Luo, Y. (2006). On the variability of respiration in terrestrial ecosystems: Moving beyond Q10. *Global Change Biology*, *12*, 154–164. https://doi.org/10.1111/j.1365-2486.2005.01065.x

Desai, A. R., Murphy, B. A., Wiesner, S., Thom, J., Butterworth, B. J., Koupaei-Abyazani, N., Muttaqin, A., Paleri, S., Talib, A., Turner, J., Mineau, J., Merrelli, A., Stoy, P., & Davis, K. (2022). Drivers of Decadal Carbon Fluxes Across Temperate Ecosystems. *Journal of Geophysical Research: Biogeosciences*, *127*(12), e2022JG007014. https://doi.org/10.1029/2022JG007014

Elshall, A. S., Ye, M., Pei, Y., Zhang, F., Niu, G.-Y., & Barron-Gafford, G. A. (2018). Relative model score: A scoring rule for evaluating ensemble simulations with application to microbial soil respiration modeling. *Stochastic Environmental Research and Risk Assessment*, *32*(10), 2809–2819. https://doi.org/10.1007/s00477-018-1592-3

Falge, E., Baldocchi, D., Olson, R., Anthoni, P., Aubinet, M., Bernhofer, C., Burba, G., Ceulemans, R., Clement, R., Dolman, H., Granier, A., Gross, P., Grünwald, T., Hollinger, D., Jensen, N.-O., Katul, G., Keronen, P., Kowalski, A., Lai, C. T., … Wofsy, S. (2001). Gap filling strategies for defensible annual sums of net ecosystem exchange. *Agricultural and Forest Meteorology*, *107*(1), 43–69. https://doi.org/10.1016/S0168-1923(00)00225-2

Farrance, I., & Frenkel, R. (2012). Uncertainty of Measurement: A Review of the Rules for Calculating Uncertainty Components through Functional Relationships. *The Clinical Biochemist Reviews*, *33*(2), 49–75.

Friedlingstein, P., O'Sullivan, M., Jones, M. W., Andrew, R. M., Bakker, D. C. E., Hauck, J., Landschützer, P., Le Quéré, C., Luijkx, I. T., Peters, G. P., Peters, W., Pongratz, J., Schwingshackl, C., Sitch, S., Canadell, J. G., Ciais, P., Jackson, R. B., Alin, S. R., Anthoni, P., … Zheng, B. (2023). Global Carbon Budget 2023. *Earth System Science Data*, *15*(12), 5301–5369. https://doi.org/10.5194/essd-15-5301-2023

Hamdi, S., Moyano, F., Sall, S., Bernoux, M., & Chevallier, T. (2013). Synthesis analysis

of the temperature sensitivity of soil respiration from laboratory studies in relation to incubation methods and soil conditions. *Soil Biology and Biochemistry*, *58*, 115–126. https://doi.org/10.1016/j.soilbio.2012.11.012

Hirano, T., Kim, H., & Tanaka, Y. (2003). Long-term half-hourly measurement of soil CO2 concentration and soil respiration in a temperate deciduous forest. *Journal of Geophysical Research: Atmospheres*, *108*(D20). https://doi.org/10.1029/2003JD003766

Jackson, R. B., Lajtha, K., Crow, S. E., Hugelius, G., Kramer, M. G., & Piñeiro, G. (2017). The Ecology of Soil Carbon: Pools, Vulnerabilities, and Biotic and Abiotic Controls. *Annual Review of Ecology, Evolution and Systematics*, *48*(Volume 48, 2017), 419–445. https://doi.org/10.1146/annurev-ecolsys-112414-054234

Jian, J., Bailey, V., Dorheim, K., Konings, A. G., Hao, D., Shiklomanov, A. N., Snyder, A., Steele, M., Teramoto, M., Vargas, R., & Bond-Lamberty, B. (2022). Historically inconsistent productivity and respiration fluxes in the global terrestrial carbon cycle. *Nature Communications*, *13*(1), 1733. https://doi.org/10.1038/s41467-022-29391-5

Jian, J., Vargas, R., Anderson-Teixeira, K., Stell, E., Herrmann, V., Horn, M., Kholod, N., Manzon, J., Marchesi, R., Paredes, D., & Bond-Lamberty, B. (2021). A restructured and updated global soil respiration database (SRDB-V5). *Earth System Science Data*, *13*(2), 255–267. https://doi.org/10.5194/essd-13-255-2021

Jiang, J., Feng, L., Hu, J., Liu, H., Zhu, C., Chen, B., & Chen, T. (2024). Global soil respiration predictions with associated uncertainties from different spatio-temporal data subsets. *Ecological Informatics*, *82*, 102777. https://doi.org/10.1016/j.ecoinf.2024.102777

Jobbágy, E. G., & Jackson, R. B. (2000). The Vertical Distribution of Soil Organic Carbon and its Relation to Climate and Vegetation. *Ecological Applications*, *10*(2), 423–436. https://doi.org/10.1890/1051-0761(2000)010%5B0423:TVDOSO%5D2.0.CO;2

Liu, K., Li, X., Wang, S., & Zhang, H. (2023). A robust gap-filling approach for European Space Agency Climate Change Initiative (ESA CCI) soil moisture integrating satellite observations, model-driven knowledge, and spatiotemporal machine learning. *Hydrology and Earth System Sciences*, *27*(2), 577–598. https://doi.org/10.5194/hess-27-577-2023

Luo, Y., Ogle, K., Tucker, C., Fei, S., Gao, C., LaDeau, S., Clark, J. S., & Schimel, D. S. (2011). Ecological forecasting and data assimilation in a data-rich era. *Ecological Applications*, *21*(5), 1429–1442. https://doi.org/10.1890/09-1275.1

Maier, M., & Schack-Kirchner, H. (2014). Using the gradient method to determine soil gas flux: A review. *Agricultural and Forest Meteorology*, *192–193*, 78–95. https://doi.org/10.1016/j.agrformet.2014.03.006

Mariethoz, G., Linde, N., Jougnot, D., & Rezaee, H. (2015). Feature-preserving interpolation and filtering of environmental time series. *Environmental Modelling & Software*, *72*, 71–76. https://doi.org/10.1016/j.envsoft.2015.07.001

Marshall, T. J. (1959). The Diffusion of Gases Through Porous Media. *Journal of Soil Science*, *10*(1), 79–82. https://doi.org/10.1111/j.1365-2389.1959.tb00667.x

Millington, R. J., & Shearer, R. C. (1971). Diffusion in aggregated porous media. *Soil Science*, *111*(6), 372–378.

Moffat, A. M., Papale, D., Reichstein, M., Hollinger, D. Y., Richardson, A. D., Barr, A. G., Beckstein, C., Braswell, B. H., Churkina, G., Desai, A. R., Falge, E., Gove, J. H., Heimann,

M., Hui, D., Jarvis, A. J., Kattge, J., Noormets, A., & Stauch, V. J. (2007). Comprehensive comparison of gap-filling techniques for eddy covariance net carbon fluxes. *Agricultural and Forest Meteorology*, *147*(3), 209–232. https://doi.org/10.1016/j.agrformet.2007.08.011

Moldrup, P., Olesen, T., Yamaguchi, T., Schjønning, P., & Rolston, D. E. (1999). Modeling diffusion and reaction in soils: 9. The Buckingham-Burdine-Campbell equation for gas diffusivity in undisturbed soil. *Soil Science*, *164*(2), 75.

National Ecological Observatory Network (NEON). (2024a). *Barometric pressure (DP1.00004.001).* National Ecological Observatory Network (NEON). https://doi.org/10.48443/RT4V-KZ04

National Ecological Observatory Network (NEON). (2024b). *Soil CO2 concentration (DP1.00095.001).* National Ecological Observatory Network (NEON). https://doi.org/10.48443/E7GR-6G94

National Ecological Observatory Network (NEON). (2024c). *Soil physical and chemical properties, Megapit (DP1.00096.001).* National Ecological Observatory Network (NEON). https://doi.org/10.48443/S6ND-Q840

National Ecological Observatory Network (NEON). (2024d). *Soil temperature (DP1.00041.001).* National Ecological Observatory Network (NEON). https://doi.org/10.48443/Q24X-PW21

National Ecological Observatory Network (NEON). (2024e). *Soil water content and water salinity (DP1.00094.001).* National Ecological Observatory Network (NEON). https://doi.org/10.48443/A8VY-Y813

Norman, J. M., Kucharik, C. J., Gower, S. T., Baldocchi, D. D., Crill, P. M., Rayment, M., Savage, K., & Striegl, R. G. (1997). A comparison of six methods for measuring soil-surface carbon dioxide fluxes. *Journal of Geophysical Research: Atmospheres*, *102*(D24), 28771–28777. https://doi.org/10.1029/97JD01440

Phillips, C. L., Bond-Lamberty, B., Desai, A. R., Lavoie, M., Risk, D., Tang, J., Todd-Brown, K., & Vargas, R. (2017). The value of soil respiration measurements for interpreting and modeling terrestrial carbon cycling. *Plant and Soil*, *413*(1), 1–25. https://doi.org/10.1007/s11104-016-3084-x

Raftery, A. E., Gneiting, T., Balabdaoui, F., & Polakowski, M. (2005). *Using Bayesian Model Averaging to Calibrate Forecast Ensembles.* https://doi.org/10.1175/MWR2906.1

Sallam, A., Jury, W. A., & Letey, J. (1984). Measurement of Gas Diffusion Coefficient under Relatively Low Air-filled Porosity. *Soil Science Society of America Journal*, *48*(1), 3–6. https://doi.org/10.2136/sssaj1984.03615995004800010001x

Shao, J., Zhou, X., Luo, Y., Li, B., Aurela, M., Billesbach, D., Blanken, P. D., Bracho, R., Chen, J., Fischer, M., Fu, Y., Gu, L., Han, S., He, Y., Kolb, T., Li, Y., Nagy, Z., Niu, S., Oechel, W. C., … Zhang, J. (2015). Biotic and climatic controls on interannual variability in carbon fluxes across terrestrial ecosystems. *Agricultural and Forest Meteorology*, *205*, 11–22. https://doi.org/10.1016/j.agrformet.2015.02.007

Shao, P., Zeng, X., Moore, D. J. P., & Zeng, X. (2013). Soil microbial respiration from observations and Earth System Models. *Environmental Research Letters*, *8*(3), 034034. https://doi.org/10.1088/1748-9326/8/3/034034

Sihi, D., Gerber, S., Inglett, P. W., & Inglett, K. S. (2016). Comparing models of microbial–substrate interactions and their response to warming. *Biogeosciences*, *13*(6), 1733–1752.

https://doi.org/10.5194/bg-13-1733-2016

Tang, J., Baldocchi, D. D., Qi, Y., & Xu, L. (2003). Assessing soil CO2 efflux using continuous measurements of CO2 profiles in soils with small solid-state sensors. *Agricultural and Forest Meteorology*, *118*(3), 207–220. https://doi.org/10.1016/S0168-1923(03)00112-6

Tang, J., Misson, L., Gershenson, A., Cheng, W., & Goldstein, A. H. (2005). Continuous measurements of soil respiration with and without roots in a ponderosa pine plantation in the Sierra Nevada Mountains. *Agricultural and Forest Meteorology*, *132*(3), 212–227. https://doi.org/10.1016/j.agrformet.2005.07.011

Taylor, J. R. (2022). *An Introduction to Error Analysis: The Study of Uncertainties in Physical Measurements, Third Edition* (3rd ed.). University Science Press.

Yan, Z., Bond-Lamberty, B., Todd-Brown, K. E., Bailey, V. L., Li, S., Liu, C., & Liu, C. (2018). A moisture function of soil heterotrophic respiration that incorporates microscale processes. *Nature Communications*, *9*(1), 2562. https://doi.org/10.1038/s41467-018-04971-6

Yan, Z., Liu, C., Todd-Brown, K. E., Liu, Y., Bond-Lamberty, B., & Bailey, V. L. (2016). Pore-scale investigation on the response of heterotrophic respiration to moisture conditions in heterogeneous soils. *Biogeochemistry*, *131*(1), 121–134. https://doi.org/10.1007/s10533-016-0270-0

Zhang, R., Kim, S., Kim, H., Fang, B., Sharma, A., & Lakshmi, V. (2023). Temporal Gap-Filling of 12-Hourly SMAP Soil Moisture Over the CONUS Using Water Balance Budgeting. *Water Resources Research*, *59*(12), e2023WR034457. https://doi.org/10.1029/2023WR034457